Modelling of fast landslides and waves induced by them in reservoirs and other water bodies

M. Pastor [1,2], M. Quecedo[2,3], M.I. Herreros[1,2], E. González[2,4],
B. Haddad[1,2], J.A. Fernández Merodo[1,2], P. Mira[1,2]

Summary

Some fast, catastrophic landslides, propagating over long distances exhibit a fluid like behaviour. Fluidization –or liquefaction- of the soil is caused by its very loose, metastable structure. Tendency to densify under shearing generates the high pore pressures responsible of this phenomenon. We propose a general model for the coupling between solid skeleton and the pore fluids, which can be used both for initiation and propagation phases. The model is able to simulate dissipation of pore pressures at the propagation phase. From here, it is possible to simplify the model by integration in depth. If the full model is kept, it is necessary to describe the interface with the atmospheric air, which is done using a level set algorithm. An advantage of the proposed formulation is that it is also possible to model the effects of the landslide when entering a reservoir, lake or bay. There several interfaces (air-soil, air-water and soil-water) are modeled via level set also.

1. Introduction

There is a wide variety of types of landslides, depending on the materials involved and triggering mechanism. The time scale involved can range from minutes to years. The main types of landslides, according to Dikau *et al.* [1996] are the following: (i) Fall, (ii) Topple, (iii) Slides, (iv) Lateral spreading, (v) Flows, and (vi) complex movements. Here we will deal with flows mainly, which can be described as fluid like movements where individual particles travel separately. As examples of flows, it is worth mentioning flowslides in poorly compacted deposits which experiment a sudden collapse with important build up of pore pressures and liquefaction in some cases. The failure mechanism can be described as diffuse, and the moving mass does not behave like a rigid block.

It is possible to describe the whole process (initiation and propagation) using a single mathematical model. However, there exists a difficulty in the cases where the landslide evolves to flow type phenomena, where the problem of changing from solid-like to fluid-like type of behaviour presents important difficulties. This is why we will deal separately with both phases, using different approaches for them.

[1] Centro de Estudios y Experimentación de Obras Públicas (CEDEX), Madrid, Spain

[2] M^{2}i (Math. Model. Eng. Group), Dept. of Applied Mathematics
ETS Ingenieros de Caminos, UPM Madrid, Spain

[3] ENUSA, Madrid, Spain

[4] ADIF, Madrid, Spain (formerly at CEDEX)

In the initiation phase, we can consider two different mechanisms of failure: localized and diffuse. Localized failure presents important mathematical and numerical difficulties. Concerning the former, the interested reader will find in Vardoulakis and Sulem [1995] a detailed description.

The study of diffuse mechanisms is more recent, and we should mention the work of F. Darve [1991] who named it. Details could be also found in Pastor and Tamagnini [2002] and Fernández Merodo *et al.* [2003]. Many landslides presenting a clear failure surface, like rotational and translational landslides, fall in this category. Diffuse failures do not present such clear surfaces, and the mass of soil is much larger. This mechanism of failure is characteristic of soils presenting very loose or metastable structures with a strong tendency to compact under shearing. One paramount feature is that effective stresses approach zero, and the material behaves like a viscous fluid in which buildings can sink, as it happened during the 1966 earthquake of Niigata in Japan. When this failure mode takes place in a slope, the mass of mobilized soil can propagate downhill, evolving into flow slides or mudflows. Therefore, using a proper constitutive model is crucial. Of course, there will be mixed types where an initial localized mechanism evolves into a diffuse mode as masses of soil liquefy.

A special case is that of landslides occuring on slopes of reservoirs, lakes, bays, etc. Depending on the circumstances, a large wave can be generated such that its effects can devastate villages on the banks or even downstream of the dam, as happened in the well known case of Vaiont. We will show here that models developed for propagation of fast cata-

strophic landslides can be applied to predict the wave generated by them and its effects.

2. Mathematical Model

The first mathematical model describing the coupling between solid and fluid phases was proposed by BIOT [1941, 1955] for linear elastic materials. This work was followed by further development at Swansea University, where ZIENKIEWICZ and coworkers [1984, 1990a, 1990b, 2000] extended the theory to non-linear materials and large deformation problems. It is also worth mentioning the work of LEWIS and SCHREFLER [1998], COUSSY [1995] and DE BOER [2000]. It can be concluded that the geotechnical community has incorporated coupled formulations to describe the behaviour of foundations and geostructures. Indeed, analyses of earth dams, slope failures and landslide triggering mechanisms have been carried out using such techniques during last decades.

2.1. General model

We will assume that soil consists of a solid skeleton and several fluid phases. The soil skeleton consists of particles of density ρ_s having a porosity n (volume percent of voids in the mixture). The voids can be filled with air and water, but in some cases there will be mixtures of water and very fine particles which can be considered as a fluid phase.

We will assume that fluid phases (α) are not miscible, defining S_α as the degree of saturation for the phase α, i.e., the volume fraction of voids occupied by it. In the case of air and water, we will define S_w and S_a as the volume fractions occupied by water and air. We will introduce $\rho^{(\alpha)}$ to denote the density of the phase (α). If the fluid density is ρ_α we will have for the mixture constituents ρ_α, $\rho^{(\alpha)} = nS_\alpha\rho_\alpha$ and $\rho^{(s)} = (1-n)\rho_s$.

If we denote by $\sigma^{(s)}$ and $\sigma^{(\alpha)}$ the Cauchy stress tensors acting on the solid particles and on the phase (α), we can define the partial stresses $\sigma^{(s)}$ and $\sigma^{(\alpha)}$ as $\sigma^{(s)} = (1-n)\sigma_s$ and $\sigma^{(\alpha)} = nS_\alpha\sigma_\alpha$. The total stress tensor is given by:

$$\sigma = \sigma^{(s)} + \sum_{\alpha=1}^{\text{nphases}} \sigma^{(\alpha)} \tag{1}$$

The partial stresses $\sigma^{(\alpha)}$ can be decomposed into hydrostatic and deviatoric components as $\sigma^{(\alpha)} = -nS_\alpha p_\alpha \mathtt{I} + nS_\alpha s_\alpha$ where $s_\alpha = \text{dev}(\sigma_\alpha)$ is the deviatoric part of $\sigma^{(\alpha)}$ and $\mathtt{I}$ is the identity tensor of second order. It is important to note that if the saturating fluid is water, the deviatoric stresses can be neglected, but in other cases where viscous contributions are important, this term has to be taken into account. In above we have assumed that tractions are positive. We will also define the averaged pore pressure p– as

$$\bar{p} = \sum_{\alpha=1}^{\text{nphases}} p^{(\alpha)} = \sum_{\alpha=1}^{\text{nphases}} S_\alpha p_\alpha \tag{2}$$

The equations of balance for the solid skeleton and the fluid phases are given by:

(a1) Balance of mass for solid and interstitial fluids:

$$\begin{aligned} \frac{D^{(s)}\rho^{(s)}}{Dt} + \rho^{(s)} \text{div}\, \mathbf{v}^{(s)} = 0 \\ \frac{D^{(\alpha)}\rho^{(\alpha)}}{Dt} + \rho^{(\alpha)} \text{div}\, \mathbf{v}^{(\alpha)} = 0 \end{aligned} \tag{3}$$

(a2) Balance of linear momentum for the fluids

$$\rho^{(\alpha)} \frac{D^{(\alpha)} v^{(\alpha)}}{Dt} = \rho^{(\alpha)} b + \text{div}\,\sigma^{(\alpha)} - k_\alpha^{-1} w^{(\alpha)} \tag{4}$$

and the solid skeleton

$$\rho^{(s)} \frac{D^{(s)} v^{(s)}}{Dt} = \rho^{(s)} b + \text{div}\,\sigma^{(s)} - k_\alpha^{-1} w^{(\alpha)} \tag{5}$$

where **b** are the body forces, k_α the permeability tensor of phase α, and $w^{(\alpha)}$ the Darcy's velocity $\omega^{(\alpha)} = nS_\alpha (v^{(\alpha)} - v^{(s)})$.

In above we have introduced the total derivatives of a magnitude ϕ following phase $^{(\alpha)}$ or the solid skeleton as:

$$\frac{D^{(\alpha)}\phi}{Dt} = \frac{\partial\phi}{\partial t} + v^{(\alpha)} . \text{grad}\,(\phi)$$

(a3) Constitutive equations for all phases relating stresses or their increments to strain or strain rate tensors. In the case of solids, elastic, elastoplastic or viscoplastic models are commonly used, while the fluids are modeled using Newtonian, Bingham, Bagnold, or frictional fluid models.

(a4) Finally, the model is completed with equations relating displacements or velocities to strain or rate of strain tensors.

The model described above is general, and can be applied to a wide variety of phenomena. In what follows, we propose two simplifications: (1) in some cases it is possible to consider one single phase. This is the case of mudflows and the avalanches of granular materials. (2) in the case of flowslides, we will assume that the movement of the fluid phase relative to the soil skeleton is not large. We will use the so called "u-pw" model proposed by Zienkiewicz, and a variant of it in terms of velocities. Then, we will average in depth the equations. This will be described next. It is important to re-

mark that in all cases considered in this paper we have used an eulerian approach.

2.2. Swansea model: the u-pw formulation

If we assume that velocities and accelerations of fluids relative to solid skeleton are small, the model can be cast in terms of velocity of the solid skeleton and Darcy's velocities of pore fluids. If we further assume that the soil is unsaturated with an air pressure equal to zero, the resulting model consists of the following equations:

(i) Balance of mass and momentum of pore water, which is obtained eliminating the Darcy's velocity of the pore water:

$$\operatorname{div} v + \operatorname{div}\left\{\frac{k_w}{S_w}\left(-\rho_w \frac{Dv}{Dt} + \rho_w b - \operatorname{grad} p_w + \operatorname{div} S_w\right)\right\} + \frac{1}{Q}\frac{Dp_w}{Dt} + \frac{1}{G}\frac{DS_w}{Dt} = 0$$

where

$$\frac{1}{Q} = \left[\frac{1-n}{K_s} + \frac{n}{K_w}\right] \text{ and } \frac{1}{G} = \left[\frac{1-n}{K_s} p_w + \frac{n}{S_w}\right] \qquad (6)$$

(ii) Balance of momentum of the mixture

$$\rho \frac{D^{(s)} v^{(s)}}{Dt} = \rho b + \operatorname{div} \sigma \qquad (7)$$

These equations are complemented with a suitable constitutive equation and with a kinematical relation linking displacements (or velocities) to strains. Divergence of accelerations and body forces are often neglected in geotechnical engineering. This model, cast in terms of velocities instead of displacements, is the much celebrated displacement pressure (u-pw) model proposed by ZIENKIEWICZ and coworkers at Swansea University [ZIENKIEWICZ, 1984].

2.3. A propagation-consolidation model

So far we have described general models which can be applied to general problems in soil mechanics. The analysis of landslides, due to their shape and geometrical properties allow some interesting simplifications. First of all, we will arrive to "propagation-consolidation" models, where pore pressure dissipation takes place along the normal to the terrain surface, and next, we will describe depth integrated models, where the three dimensional problem is transformed into a two dimensional form. The starting point is the balance equations for a saturated soil obtained above:

$$\rho \frac{D^{(s)} v^{(s)}}{Dt} = \rho b + \operatorname{div} \sigma$$

$$\operatorname{div}(-k_w \operatorname{grad} p_w) + \operatorname{div} v^s = 0$$

where we have neglected the term $\frac{1}{Q}\frac{Dp_w}{Dt}$.

These equations are completed with the constitutive/rheological equations and the kinematical relations relating strains and their rate to displacements or velocities.

One important aspect is that fast landslides involve two physical phenomena which appear in above equations: (i) consolidation and dissipation of pore pressures, and (ii) propagation. In order to gain insight on the relative importance of all terms, we will express above equations in non-dimensional form as proposed by Hutter and Koch [1991], introducing a characteristic length of the landslide L and H a characteristic depth of the sliding mass, and the ratio $\varepsilon = H/L$. In typical cases, L will be of the order of 10^2m and H of the order of 5 m. Therefore, ε will be small.

We will introduce next some characteristic magnitudes of the slide. First, we will use L as a characteristic length, and H a characteristic depth of the flow. In most cases, the ratio $\varepsilon = H/L$ can be assumed to be small (shallow landslides). The time scale is $T = (L/g)$, and a typical velocity $v = (gL)$. Finally, the stresses and pressures will be compared to the reference pressure $\rho_0 gH$, where ρ_0 is a reference density. The x_1 and x_2 axes will be chosen on a plane close to that of the slope, or a horizontal one, and the x_3 axis will be normal to this plane. The v-p_w model can be cast in a non dimensional form by introducing

$$\hat{x}_1 = x_1/L \qquad \hat{x}_2 = x_2/L \qquad \hat{x}_3 = x_3/L$$
$$\hat{v}_1 = v_1/\sqrt{gL} \qquad \hat{v}_2 = v_2/\sqrt{gL} \qquad \hat{v}_3 = \varepsilon v_3/\sqrt{gL}$$
$$\hat{\sigma} = \sigma/\rho_0 gH \qquad \hat{p}_w = p_w/\rho_0 gH$$

The non dimensional form of the balance of mass and momentum can be written as:

$$\operatorname{div} \hat{v} = \theta\left(\varepsilon^2 \frac{\partial^2 \hat{p}_w}{\partial \hat{x}_1^2} + \varepsilon^2 \frac{\partial^2 \hat{p}_w}{\partial \hat{x}_2^2} + \frac{\partial^2 \hat{p}_w}{\partial \hat{x}_3^2}\right) \qquad (8)$$

which reduces to

$$\operatorname{div} \hat{v} = \theta \frac{\partial^2 \hat{p}_w}{\partial x_3^2} \qquad (9)$$

for shallow landslides. In above, we have introduced the non dimensional magnitude θ given by

$$\theta = \left(\frac{\sqrt{L/g}}{H/(k_w \rho_0 g)}\right) \qquad (10)$$

Assuming the same typical values for L and H, and a permeability such that $k_w \rho_0 g$ is of the order of 10^{-n} ms^{-1}, it can be seen that θ will be close to 10^{-n}. Typical values are 10^{-9} for clays, 10^{-7} for silts, 10^{-5} for fine sands and 10^{-1} for gravels.

The component along x_3 of the balance of momentum equation for the mixture results in

$$\varepsilon\left\{\frac{\partial \hat{u}_3}{\partial \hat{t}}+\text{grad}\,\hat{u}_3.\hat{u}\right\}=-1+\left[\varepsilon\frac{\partial \hat{\sigma}_{13}}{\partial \hat{x}_1}+\varepsilon\frac{\partial \hat{\sigma}_{23}}{\partial \hat{x}_2}+\frac{\partial \hat{\sigma}_{33}}{\partial \hat{x}_3}\right] \quad (11)$$

where we have assumed that gravity acts along the axis x_3, and therefore, $\hat{b}_3 = -\hat{g} = -1$. If we assume that ε is small, above equation reduces to

$$-1+\frac{\partial \hat{\sigma}_{33}}{\partial \hat{x}_3}=0$$

Or, in terms of effective stresses:

$$-1+\frac{\partial \hat{\sigma}'_{33}}{\partial \hat{x}_3}-\frac{\partial \hat{p}_w}{\partial \hat{x}_3}=0$$

From here, the dimensional equations are:

$$\begin{aligned} &\text{div}\, v=\frac{\partial}{\partial x_3}\left(k_w\frac{\partial p_w}{\partial x_3}\right)\\ &-\rho g+\frac{\partial \sigma_{33}}{\partial x_3}=0\\ &-\rho g+\frac{\partial \sigma'_{33}}{\partial x_3}-\frac{\partial p_w}{\partial x_3}=0 \end{aligned} \quad (12)$$

We will assume next that the velocity field can be decomposed as

$$\hat{v}=\hat{v}_0+\hat{v}_1 \quad (13)$$

and the pore pressure field will be assumed to be of the form

$$\hat{p}_w=\hat{p}_{w0}+\hat{p}_{w1} \quad (14)$$

where p_{w0} is a hydrostatic field varying linearly from zero at the surface to ρgh at the bottom. From here we obtain

$$\text{div}\,\hat{v}_0+\text{div}\,\hat{v}_1=\theta\left(\frac{\partial^2 \hat{p}_{w0}}{\partial \hat{x}_3^2}+\frac{\partial^2 \hat{p}_{w1}}{\partial \hat{x}_3^2}\right)=\theta\frac{\partial^2 \hat{p}_{w1}}{\partial \hat{x}_3^2} \quad (15)$$

And we will assume

$$\begin{aligned} &\text{div}\,\hat{v}_0=0\\ &\text{div}\,\hat{v}_1=\theta\frac{\partial^2 \hat{p}_w}{\partial \hat{x}_3^2} \end{aligned} \quad (16)$$

In this way, we can identify the perturbed field v_1 as the velocity field corresponding to consolidation and v_0 as the velocity field corresponding to propagation. This result is of paramount importance, and clarifies the assumptions which should be made when modelling these phenomena. First of all, incompressibility is not a feature of rheological soil behaviour, but a consequence of the coupled behaviour between the pore fluid and the soil skeleton. Indeed, this will explain the "undrained" behavior in simple shear devices, where pressures depend on shear strain rate.

If we now approximate the divergence as

$$\text{div}\, v_1=\frac{1}{K_T}\frac{Dp_w}{Dt} \quad (17)$$

where K_T is the volumetric stiffness modulus of soil skeleton, we arrive to

$$\frac{1}{K_T}\frac{Dp_w}{Dt}=\frac{\partial}{\partial x_3}\left(k_w\frac{\partial p_w}{\partial x_3}\right) \quad (18)$$

where p_w depends on x_1, x_2, x_3 and t.

2.4. Depth integrated models

The model describing the propagation phase obtained in the preceding section consists of the following set of PDE's

$$\begin{aligned} &\rho\frac{Dv_0}{Dt}=\rho b+\text{div}\,\sigma\\ &\text{div}\, v_0^{(s)}=0 \end{aligned} \quad (19)$$

$$\frac{1}{K_T}\frac{Dp_w}{Dt}=\frac{\partial}{\partial x_3}\left(k_w\frac{\partial p_w}{\partial x_3}\right) \quad (20)$$

In what follows, we will drop the subindexes "0" and "1" which have been used to decompose the movement into propagation and consolidation. Taking into account the incompressibility condition we can write the conservative form:

$$\rho\frac{\partial v_i}{\partial t}+\frac{\partial}{\partial x_j}(\rho v_i v_j)=\frac{\partial}{\partial x_j}(\sigma_{ij})+\rho b_i$$

In certain cases, as in the case of debris flows, there exist turbulent fluctuations over averaged states. The equations are then averaged over a representative time length T, and an extra term σ_{ij}^R

$$\sigma_{ij}^R=-\frac{1}{T}\int_t^{t+T}(\rho v_i' v_j')\,dt \quad (20b)$$

is added to the stresses. In above, v'_i represents the fluctuations of the velocity v_i over the average $\bar{v}_i$. We will assume that the stress tensor σ_{ij} can include Reynolds stresses in all cases where they could be important, although in granular flows they are not so.

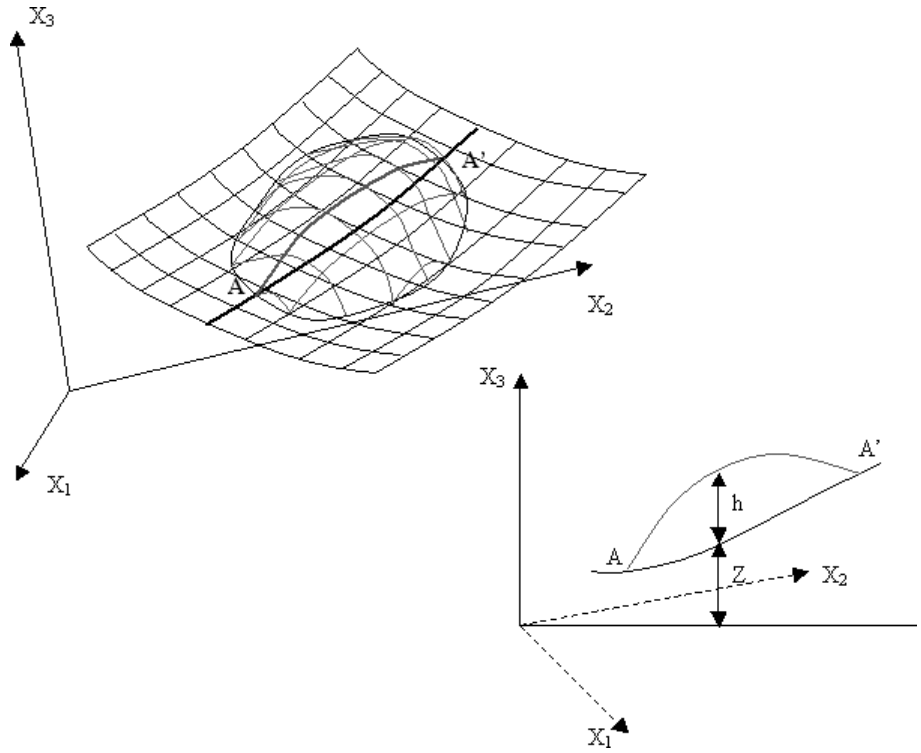

Fig. 1 – Reference system and notation used in the analysis.
Fig. 1 – Sistema di riferimento e notazione adottata nell'analisi.

For the sake of simplicity we will drop the overbar, assuming that all magnitudes are the averaged values.

The equations of the depth averaged model are obtained integrating along X3 the balance of mass and momentum equations, and taking into account Leibnitz's rule.

We will use the reference system given in Figure 1 where we have depicted some magnitudes of interest which will be used in this section.

If we integrate along X_3 the propagation submodel, we arrive to:

$$\frac{\partial h}{\partial t}+\frac{\partial}{\partial x_j}(h\bar{v}_j)=0 \quad \text{with } j=1,2 \tag{21}$$

where v_j is the depth-averaged velocity along X, and

$$\begin{aligned}&\rho\frac{\partial}{\partial t}(h\bar{v}_i)+\rho\frac{\partial}{\partial x_j}(h\bar{v}_i\bar{v}_j)=\\&=\rho b_i h+\frac{\partial}{\partial x_j}(h\bar{\sigma}_{ij})+t_i^A+t_i^B \quad \text{with } j=1,2\end{aligned} \tag{22}$$

where t_i^A and t_i^B are the surface forces at the surface and the bottom respectively,

$$\begin{aligned}t_i^A&=\sigma_{ij}\cdot n_j\big|_{z+h}\\t_i^B&=\sigma_{ij}\cdot n_j\big|_{z}\end{aligned} \tag{23}$$

and σ_{ij} is the stress tensor averaged over depth.

Depth integrated equations can be cast in conservative form as:

$$\frac{\partial U}{\partial t}+\frac{\partial F_i}{\partial x_i}=S \tag{24}$$

where

$$\begin{aligned}U^T&=(h,h\bar{v}_1,h\bar{v}_2)\\F_1^T&=(h\bar{v}_1,h\bar{v}_1^2,h\bar{v}_2^2)\\F_2^T&=(h\bar{v}_2,h\bar{v}_1\bar{v}_2,h\bar{v}_2^2)\end{aligned} \tag{25}$$

and

$$S=\begin{pmatrix}0\\b_1h\\b_2h\end{pmatrix}+\frac{1}{\rho}\left[\frac{\partial}{\partial x_1}\begin{pmatrix}0\\h\bar{\sigma}_{11}\\h\bar{\sigma}_{12}\end{pmatrix}+\frac{\partial}{\partial x_2}\begin{pmatrix}0\\h\bar{\sigma}_{12}\\h\bar{\sigma}_{22}\end{pmatrix}+\begin{pmatrix}0\\t_{1A}+t_{1B}\\t_{2A}+t_{2B}\end{pmatrix}\right] \tag{26}$$

Concerning the vertical consolidation equation, it can be integrated along X_3 also, resulting on

$$\frac{\partial}{\partial t}(\bar{p}_w h)+\frac{\partial}{\partial x_i}(\bar{v}_i\bar{p}_w h)=c_v\frac{\partial p_w}{\partial x_3}\bigg|_{z+h}-c_v\frac{\partial p_w}{\partial x_3}\bigg|_{z} \tag{27}$$

We will assume that pore pressure can be approximated by

$$p_w(x_1,x_2,x_3,t)=\sum_{j=1}^{nf}N_j^{(3)}(x_3)p_{wj}(x_1,x_2,t) \tag{28}$$

where $N_j^{(3)}(x_3)$ are shape functions used to approximate the variation of pore pressure along x_3. We will choose harmonic functions satisfying boundary conditions. If we assume that pore pressure is zero at the surface and the bottom is impervious,

$$N_j^{(3)}(x_3)=\cos\left(\frac{2j-1}{2h}\pi(x_3-z)\right) \quad j=1...nf \tag{29}$$

If we limit the analysis to a single Fourier component, we obtain

$$\frac{\partial}{\partial t}(P_{w1}h)+\frac{\partial}{\partial x_k}(\bar{v}_k P_{w1}h)=-\frac{\pi^2}{4h}c_v P_{w1} \tag{30}$$

where P_{wj} depends on x_1, x_2 and t. This equation is incorporated into the general model (24) adding one more term to the unknowns, fluxes and sources. Therefore, the system can be cast as

$$\frac{\partial U}{\partial t}+\frac{\partial F_j}{\partial x_j}=S \tag{31}$$

where

$$\begin{aligned} U^T&=(h,h\bar{v}_1,h\bar{v}_2,hP_{w1})\\ F_1^T&=(h\bar{v}_1,h\bar{v}_1^2,h\bar{v}_2\bar{v}_1,hP_{w1}\bar{v}_1)\\ F_2^T&=(h\bar{v}_2,h\bar{v}_1\bar{v}_2,h\bar{v}_2^2,hP_{w1}\bar{v}_2) \end{aligned} \tag{32}$$

and

$$\begin{aligned} S=&\begin{pmatrix}0\\ b_1h\\ b_2h\\ 0\end{pmatrix}+\frac{1}{\rho}\frac{\partial}{\partial x_1}\begin{pmatrix}0\\ h\bar{\sigma}_{11}\\ h\bar{\sigma}_{12}\\ 0\end{pmatrix}+\frac{1}{\rho}\frac{\partial}{\partial x_2}\begin{pmatrix}0\\ h\bar{\sigma}_{12}\\ h\bar{\sigma}_{22}\\ 0\end{pmatrix}+\\ &+\frac{1}{\rho}\begin{pmatrix}0\\ t_{1A}+t_{1B}\\ {}_{2A}+t_{2B}\\ 0\end{pmatrix}+\begin{pmatrix}0\\ 0\\ 0\\ -\frac{\pi^2}{4h}c_v P_{w1}\end{pmatrix} \end{aligned} \tag{33}$$

It is important to notice that consolidation results in a source term which is incorporated into the system.

2.5. A note on reference systems

In the depth integrated model the flow velocities are parallels to the plane x_1, x_2. However, fast flows propagate downhill on curved beds with big gradients, flow velocities are parallel to the bed of the slide. Changes of gradient slope and curvature produce a pore pressure distribution different to the hydrostatic one, therefore these effects must be incorporated to the general equations.

A one dimensional lagrangian model that takes into account the slope and curvature effect was proposed by SAVAGE and HUTTER [1991]. They showed that the curvature effect leads to a vertical stress increment, above all in granular materials.

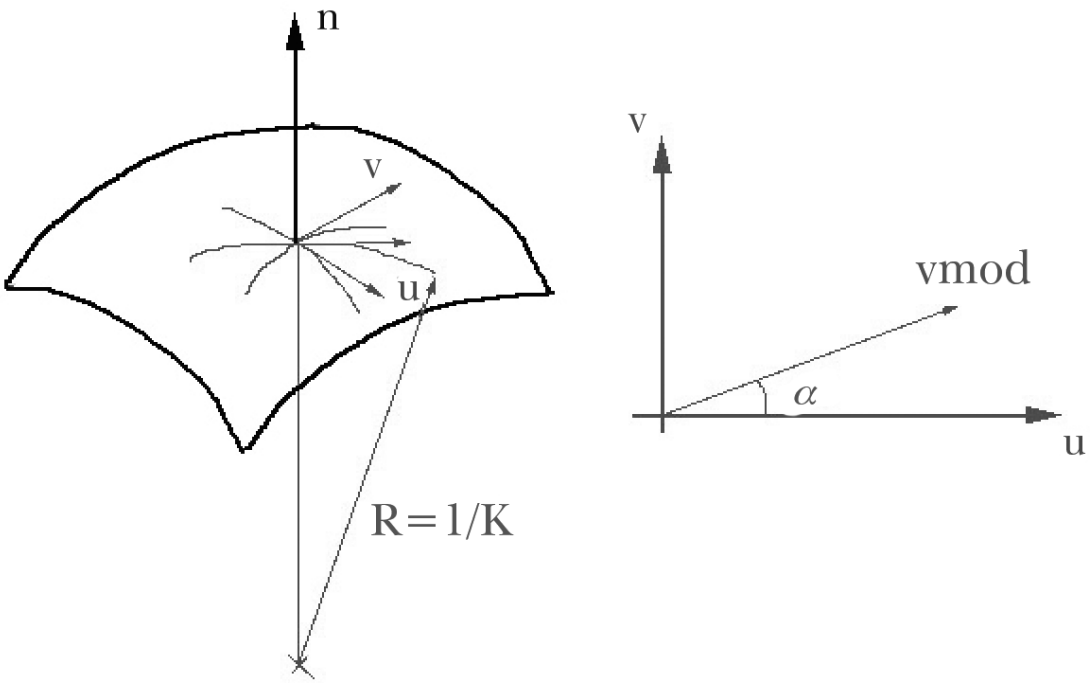

Fig. 2 – Curvature approximation.
Fig. 2 – Approssimazione della curvatura.

The movement equations were also solved by HUNGR [1995] using a lagrangian finite differences scheme. The mass was divided in a number of blocks in contact each others, which could deformate during the propagation. The curvature effect was incorporated into the bottom friction force adding to the normal component, the contribution of the centrifugal force.

If a frictional material is considered, the curvature effect can be taken into account through the two methods based on the models of SAVAGE and HUTTER and HUNGR. The first method uses a curvilinear reference system oriented in the normal and tangent directions in relation to the bed line in each point. This reference system has been used by QUECEDO and PASTOR [2003] in order to model depth integrated equations using an eulerian formulation. The second one incorporates the curvature effect in the friction law, adding to the normal force the centrifugal force. It should be remarked that this term appears in a natural way when the natural coordinate system is used.

In the simplified method, the formulation used for the friction law is:

$$|t_B| = \rho\left(g + \frac{v^2}{R}\right) h \cdot \mathrm{tg}\,\phi \tag{34}$$

In order to calculate the curvature radius R in the point M of the surface, Figure 2, the approximation is:

$$K = \frac{1}{R} = \left.\frac{d^2\bar{r}}{ds^2}\right|_M = \frac{L\cos^2\alpha + M\cos\alpha\,\mathrm{sen}\alpha + N}{E\cos^2\alpha + F\cos\alpha\,\mathrm{sen}\alpha + G} = \frac{L + M\lambda + N\lambda^2}{E + F\lambda + G\lambda^2} \tag{35}$$

where:

$$\lambda = \mathrm{tg}\alpha,\ L = \bar{n}X_{uu},\ M = \bar{n}X_{uv},\ N = \bar{n}X$$
$$E = X_u X_u,\ F = X_u X_v,\ G = X_v X_v \tag{36}$$

And if we choose ux and vy, we obtain:

$$\bar{n} = \frac{(-Z_x, -Z_y, 1)}{\sqrt{1 + Z_x^2 + Z_y^2}}$$

$$X_u = (1, 0, Z_x) \quad X_v = (0, 1, Z_y)$$

$$X_{uu} = (0, 0, Z_{xx}) \quad X_{uv} = (0, 0, Z_{xy}) \quad X$$

and the values of E, F, G, L, M and N, are:

$$E = (1 + Z_x^2) \quad F = (Z_x Z_y) \quad G = (1 + Z_y^2)$$

$$L = \frac{Z_{xx}}{\sqrt{1 + Z_x^2 + Z_y^2}} \quad M = \frac{Z_{xy}}{\sqrt{1 + Z_x^2 + Z_y^2}} \quad N = \frac{Z_{yy}}{\sqrt{1 + Z_x^2 + Z_y^2}}$$

3. Modelling of free surfaces via level set technique

One of the main problems found in the propagation phase is the proper modeling of the interfaces which separate the moving mass of soil from the atmospheric air –or the water, in the case of landslides propagating inside water bodies.

We have used a level set technique for three phases, which will be described next.

Considering that the three fluids are immiscible, the unsteady flow of the three interacting fluids: air, water and the fluid-like mass of soil is modelled using the Navier-Stokes equations:

$$\rho\frac{\partial\bar{u}}{\partial t} + \rho\, div(\bar{u}\otimes\bar{u}) = div\boldsymbol{\tau} + grad\, p + \rho\bar{b}$$
$$div\,\bar{u} = 0 \tag{37}$$

where:

- $\rho(\bar{x},t)$ is the density field
- $\bar{u}(\bar{x},t)$ is the fluid velocity
- $\bar{u}\otimes\bar{u} = u_i u_j$
- $p(\bar{x},t)$ is the pressure
- $\boldsymbol{\tau}(\bar{x},t)$ is the viscous stress tensor. It will be defined as a function of the strain rate tensor **D** later.
- $\bar{b}$ is the body force. In this case, the gravity. Other forces as surface tension at the fluids interface and Coriolis force are ignored in this paper.

Note that in the multi-fluid flow case, the continuity equation is written as $div\,\bar{u}$ instead of $div\,\rho\bar{u}$ see, for instance, LAKEHAL (2002) for the derivation.

In the proposed approach, an indicator function, $\varphi(\bar{x},t)$ identifies the portion of the domain occupied by each fluid such as depicted in Figure 3 for

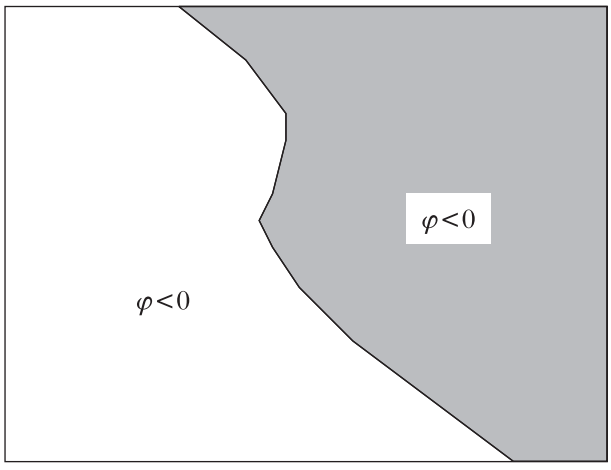

Fig. 3 – Example of description of two phases using one indicator function.
Fig. 3 – Esempio di descrizione di due fasi usando una sola funzione indice.

the simple case of two fluids, and the material properties, such as the density, may be calculated as

$$MP(\bar{x},t)=MP_1+(MP_2-MP_1)H(\varphi(\bar{x},t))$$

where MP_i is a material property (density, viscosity, yield strength,..) of fluid i and

$$H(\varphi)=\begin{cases}0 & if \quad \varphi\le 0\\ 1 & if \quad \varphi>0\end{cases}$$

This idea may be extended to the three-fluid flow case by incorporating a second indicator function, $\psi(x-,t)$, and the sub-domains occupied by each fluid identified as depicted in Figure 4.

Now, the material properties may be calculated from φ and ψ as

$$\begin{aligned}\mathrm{MP}(\bar{x},\mathrm{t})=\mathrm{MP_a}+(\mathrm{MP_w}-\mathrm{MP_a})\,\mathrm{H}(\varphi(\bar{x},\mathrm{t}))\\ +(\mathrm{MP_s}-\mathrm{MP_a})\,\mathrm{H}(\Psi(\bar{x},\mathrm{t}))\end{aligned}\qquad(38)$$

where the subscript a, w and s stands for air, water and soil respectively.

Since MP is a material property moving with the flow, its material derivative is zero

Considering now the dependence of the material properties on the indicator functions, equation (38), this condition may be written as

$$\begin{aligned}\frac{D\varphi}{Dt}&=\frac{\partial\varphi}{\partial t}+\bar{u}\,grad\,\varphi=0\\ \frac{D\psi}{Dt}&=\frac{\partial\psi}{\partial t}+\bar{u}\,grad\,\psi=0\end{aligned}\qquad(39)$$

which state that the indicators are purely advected by the flow and require the function H() to be smooth.

In the case φ and ψ are linear functions of their position, $\bar{x}$, their second order spatial derivative is zero and equations (39) are exact and also they are their numerical approximations. Thus, considering φ and ψ as linear, also benefits the numerical solution of (39) as the front smearing caused by low order numerical schemes or the oscillations induced

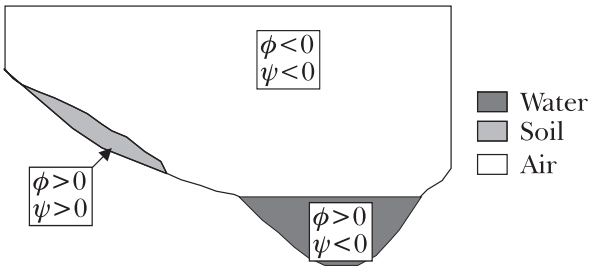

Fig. 4 – Example of description of each material subdomain using two indicator functions.
Fig. 4 – Esempio di descrizione di ogni sottodominio materiale usando due funzioni indice.

in the high order case will not appear. The simplest linear function is that with slope unity, i.e. the distance function: $grad\varphi=grad\psi=1$.

As regards the definition of H(), this equation works well only for small density ratios. For high density ratios, such as those found in the problems analyzed in this paper, $(\rho_s;\rho)/\rho_a$ 1000 it results in unwanted instabilities in the pressure field that may destroy the calculated problem solution. This problem is related to the numerical solution of a badly conditioned Poison equation for the pressure (FEDKIW 1999).

To avoid abrupt changes in the material properties when crossing the interface, they are interpolated through a constant thickness tube of total width 2δ surrounding the interface [SUSSMAN, 1994], where δ is taken of the order of the mesh size. There exist different alternatives for the definition of function H(.), such as the simple linear interpolation

$$H(\varphi)=\begin{cases}0 \ for \ \varphi\le-\delta\\ (\varphi+\delta) \ for \ -\delta<\varphi<\delta\\ 1 \ for \ \varphi\ge\delta\end{cases}$$

However, extra smoothing can be gained considering other functions. This paper considers the sine function given below [HERREROS *et al.*, 2005].

$$H(\varphi)=\begin{cases}0 \ for \ \varphi\le-\delta\\ \sin\left(\dfrac{\pi(\varphi+\delta)}{4\delta}\right) \ for \ -\delta<\varphi<\delta\\ 1 \ for \ \varphi\ge\delta\end{cases}$$

This definition of the interpolation function, based on the distance to the interface, requires keeping the indicator functions as a distance function. In effect, Equations (39) state that the indicators are advected by the fluid velocity: as the fluid velocity is not uniform in the domain, the initial distance functions will be distorted as time progresses and, after some time, they will not be any longer distance functions.

As the fluid-to-fluid interface velocity is the one advecting the interface, this issue may be solved by using the fluid flow velocity only at the interface and constructing a velocity field in the remaining domain such as it preserves compliance to the condition $grad\varphi=1$. This problem is known as the "extension problem" and the authors will back to it in next sections. Determining this new velocity field is not a simple task and algorithms to construct the extension field velocity only exists for a few problems [SETHIAN, 1996].

Another possibility is to use the fluid flow velocity as proposed in equation (39) to advect the indicators and, once the indicators are advected, to correct them to comply with the $|grad\,\varphi|=1$ condition.

This may be achieved by solving at any time t, the following problem to steady state [SUSSMAN, 1994]:

$$\frac{\partial \varphi(\hat{\tau})}{\partial \hat{\tau}} + S(\varphi(t)) \left| grad\, \varphi(\hat{\tau}) \right| = S(\varphi(t)) \qquad (40)$$

with initial conditions

$$\varphi(\bar{x}, \hat{\tau} = 0) = \varphi(\bar{x}, t)$$

where S(.) is the sign function and $\hat{\tau}$ a fictitious time.

Clearly, the steady-state solution of this problem will meet the condition $|\text{grad}\ \varphi| = 1$ and the zero level-set of $\varphi(\hat{\tau} \varnothing \infty)$ matches that of $\varphi(t)$.

Equation (40) may be written also as

$$\frac{\partial \varphi(\hat{\tau})}{\partial \hat{\tau}} + S(\varphi^n) \frac{grad\, \varphi(\hat{\tau})}{\left| grad\, \varphi(\hat{\tau}) \right|}\ grad\, \varphi(\hat{\tau}) = S(\varphi^n)$$

showing that this problem is an advection one with velocity

$$\bar{v} = S(\varphi^n) \frac{grad\, \varphi(\hat{\tau})}{\left| grad\, \varphi(\hat{\tau}) \right|}$$

This equation for the velocity indicates that the problem characteristics initiate at the interface position and travel with velocity ± 1. Therefore, reconstruction of the indicator functions as a distance function initiate at the interface position and progresses along their outward normal direction. Therefore, the critical zone, surrounding the interface position, is reconstructed in the first fictitious-time, $\hat{\tau}$, iterations of the solution of the problem (40).

4. Examples and applications

The examples and applications shown have been obtained using the codes Geoflow2D and Geoflow for propagation (full model and depth integrated model, respectively). More information can be found at the internet site of the Centre for Natural Hazards Modelling (CNH), www.cnh.caminos.upm.es.

4.1 Flowslides: the case of Aberfan

Once failure has taken place and the material attained a fluid-like state, it can propagate a high speed and reach long distances. Such was the case of Aberfan coal dump failure in 1966. The type of failure was identified as "flowslide". One of the main difficulties when modelling Aberfan flowslide is the role of pore pressures. Coal debris was a material composed of solid, fluid and gas phases, with a strong interaction between them. However, models cast in terms of effective stresses, pore pressures, and velocities of all constituents have not been used so far, because of the problem of moving interfaces mentioned above.

Depth integrated models can provide important information about runout, propagation paths and velocities, which is frequently sufficient to design protection structures. The main shortcoming of depth integrated models comes from the fact that pore fluid and solid particles are modelled as a single phase material, with properties that do not change with time. This is why Aberfan flowslide has been modelled assuming a Bingham fluid rheological law for the debris. For instance, JEYAPALAN *et al.* [1983] and JIN, FREAD [1997] obtained results which fitted well the observations choosing $\tau_y = 4794$ Pa., $\mu = 958$Pa.s and $\rho = 1760$ kg/m^3. Even if the results are good, it is possible to argue that waste coal was not fully saturated, and the material was frictional. Of course, the apparent angle of friction introduced above will be much smaller than ϕ', but vertical consolidation could have made it to change during the propagation phase. HUTCHINSON [1986] proposed a simple "sliding-consolidation" model in which it was clear that the combination of friction with basal pore pressures could provide accurate results of runout and velocities.

We will compare the method proposed in this work with the simplified analysis introduced by the authors in PASTOR *et al.* [2002]. This simplified method consists of the assumption that there exists a layer of saturated soil of height h_s on the bottom of the flowing material [HUTCHINSON, 1986]. The decrease in pore pressures is caused by vertical consolidation of this layer. Pore pressures on the top and bottom of this layer can be either estimated from the values of the vertical stresses or obtained directly from the results of finite element computations.

Assuming that the excess pore pressure evolves as

$$p_w(x_3, t) = N(x_3)\, \bar{p}_w(t)$$

it is possible to obtain a closed form solution of the consolidation equation. In the case of

$$N(x_3) = \sin\left(\frac{\pi}{2} \frac{x_3}{h_s}\right)$$

the solution is

$$\bar{p}_w(t) = \bar{p}_w^0 \exp\left(\frac{t}{T_v}\right)$$

where $T_v = \dfrac{4h_s^2}{\pi^2 c_v}$

and c_v is the coefficient of consolidation. Finally,

$$p_w(x_3, t) = \bar{p}_w^0 N(x_3) \exp\left(-\frac{t}{T_v}\right)$$

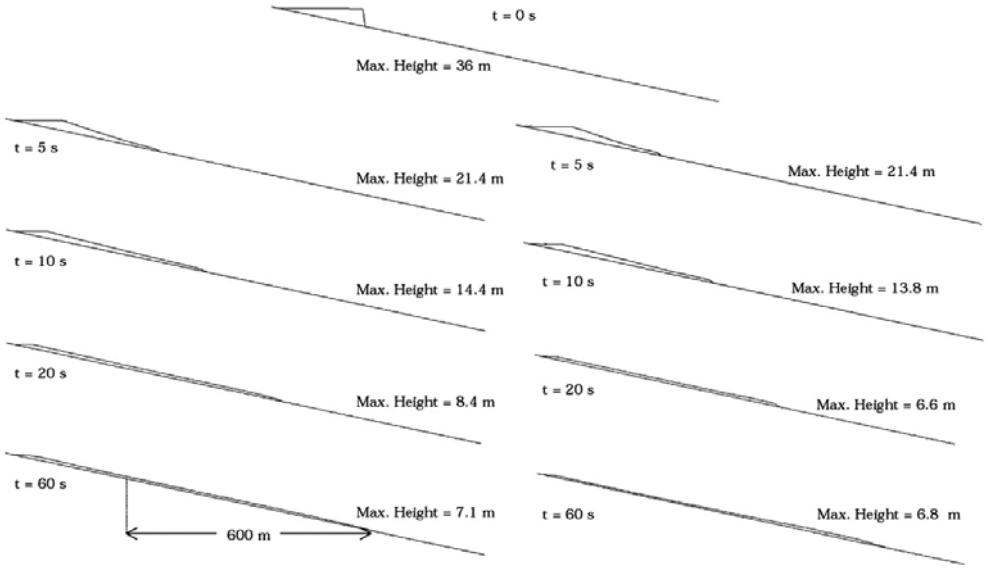

Fig. 5 – Vertical sections of Aberfan flowslide at different times (i) Left, with simplified approach for consolidation (ii) Right, enhanced method.
Fig. 5 – Sezioni verticali della frana di Aberfan a differenti istanti temporali. (i) Sinistra, approccio semplificato per la consolidazione. (ii) Destra, metodo completo.

The coefficient r_u can be estimated as:

$$r_u = r_u^0 \exp\left(\frac{t}{T_v}\right)$$

In above, we have used "pore pressures" instead of "pore water pressures". The reason is that dry or partially saturated materials can collapse generating high air pressures on their pores, which will cause a similar effect.

The information provided in the literature do not give enough data to perform a realistic analysis in two dimensions. Therefore, we have used a simple 1D model with the terrain profiles given by JEYAPALAN *et al.* [1983]. The main purpose of this example is to show that a depth integrated model using pore pressure dissipation can reproduce the basic patterns observed.

Density of the mixture ρ and friction angle ϕ', have been taken as 1740 kg/m^3 and 36º respectively. Consolidation time T_v has been estimated from the range of values proposed by Hutchinson (1986) for the depth of the saturated liquefied layer $h_s = 0.1$ m and the coefficient of consolidation $c_v = 6.410^{-5}$ m^2/s. Assuming (34), we arrive to $T_v = 64$ s. The initial value of the pore pressure coefficient r_u^0 has been taken as 0.78.

The results obtained in the simulation are given in Figure 5 where sections of the free surface of the flowslide are given at times 0, 5, 10, 20 and 60 s. On the left, we have depicted the results obtained with the simplified method. The column on the right corresponds to the method proposed in this paper. The basic features of the flow obtained in the simulation (propagation distance ≈ 600m, freezing time ≈ 40s and average velocity 15m/s) coincide reasonably well with those reported in the literature.

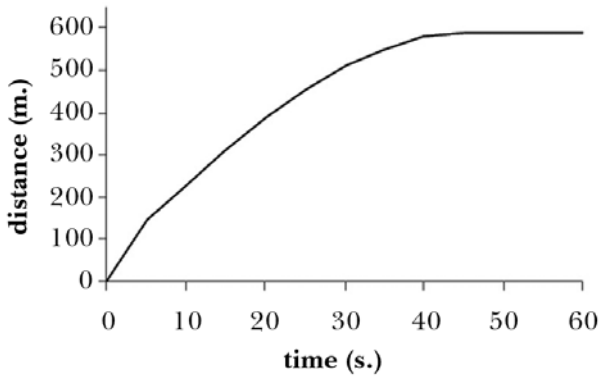

Fig. 6 – Position of head of Aberfan flowslide as a function of time.
Fig. 6 – Posizione della testa della colata di Aberfan in funzione del tempo.

Figure 6 shows position of the front as a function of time. The differences between both of the approaches are small, and affect only the profile. With the advected pore pressure, the front depth can be seen to be larger.

4.2. Flowslides: Greenhills Cougar 7 dump failure

Among of the large number of flowslides that have occurred due to liquefaction from the Rocky Mountains coal mine waste dumps, three interesting cases have been analyzed in detail by DAWSON

et al., (1998), where information on material properties can be found.

Here we will consider the case of Fording Greenhills, where in May 1992 the Cougar 7 dump failed. The mobilized mass of debris consisted of approximately 200000 m3, which slid off the 100 m high dump travelling a distance of 700 m before coming to rest.

The debris were mainly sandy gravel, and the foundation beneath the dump and the runout debris consisted of a sand and gravel colluvium layer with a depth varying between 0.3 m and 0.5 m beneath the dump. Wet fine grained layers were found at the foundation contact, near the crest, and in the debris.

According to the post failure analysis carried out by Dawson, these layers played a paramount role in both the initiation and the propagation phases. The collapse model proposed by them is based on the existence of layers of finer sandy gravel materials of low permeability deposited parallel to the dump face. Triggering mechanism could have consisted of: (i) a redistribution of effective stresses caused by pore pressure changes, and (ii) liquefaction of these layers under quasi undrained conditions. The flowslide could have ridded over these layers of liquefied materials.

The analysis of this flowslide has been based on the geotechnical properties obtained by DAWSON *et al.* [1998], and we have chosen accordingly a density of 1900 kg/m3 and an effective friction angle $\phi' = 37^{o}$. The mobilized mass has been taken from the data given in by Dawson *et al.* [1998], and the consolidation time has been chosen from back analysis equal to 68 s.

The two dimensional model of Greenhills Cougar 7 dump is given in Figure 7. The terrain model has been obtained from the data given in by DAWSON *et al.* The results of the simulation is given in Figure 8 where it can be seen perspectives of the flowslide extension.

4.3. Waves in reservoirs caused by landslides

Impulse waves in water bodies such as reservoirs, lakes or estuaries can be triggered by the impact of a sub-aerial fast landslide or a shore instability against the otherwise undisturbed water body. Due to the steep slopes that may surround the water body and the density of the material involved in the fast landslide, its velocity may be quite significant. This high velocity, a large slide mass and a narrow water body geometry, makes the potential for destruction of the generated water wave very high as it can overtop dams and destroy tailwater villages, or

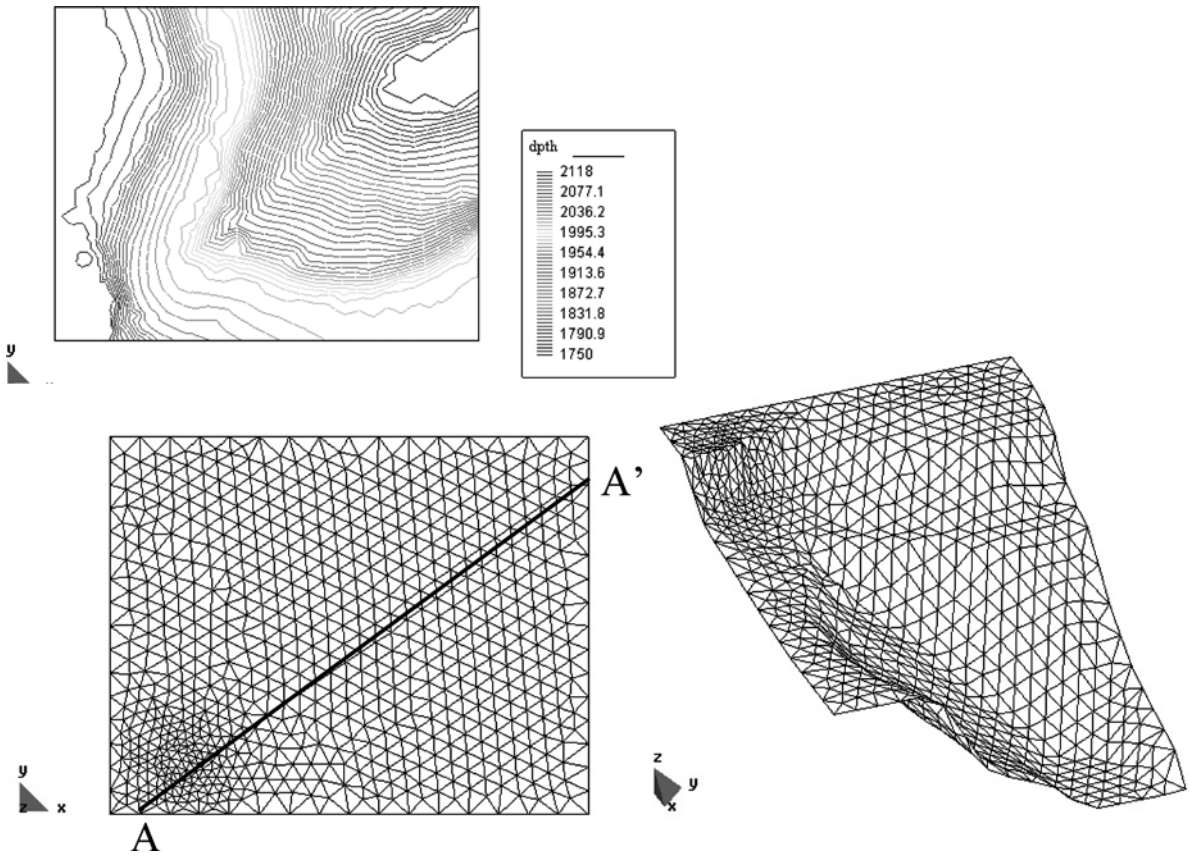

Fig. 7 – Terrain model and finite element mesh of Cougar 7 dump.
Fig. 7 – Modello del terreno e maglia a elementi finiti dello scarico Cougar 7.

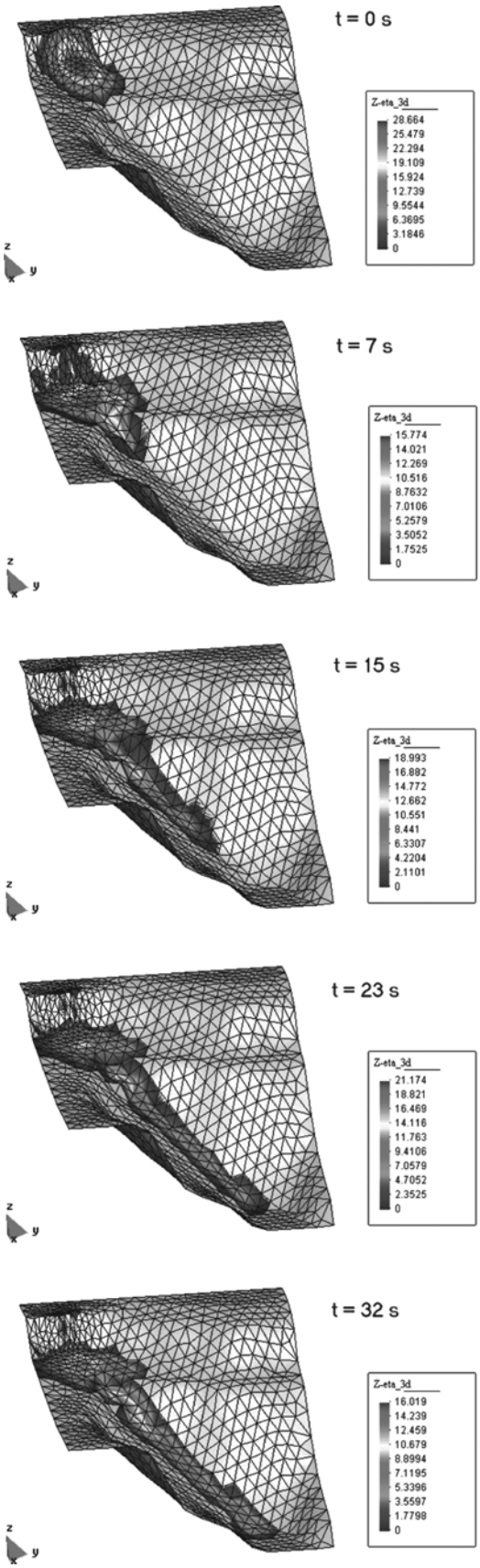

Fig. 8 – Evolution of the Greenhills Cougar 7 dump flowslide.
Fig. 8 – Evoluzione della colata allo scarico Cougar 7 delle Greenhills.

it may run up along the shore line destroying the villages located at the shore.

As an example, the Vaiont disaster in 1963 involved the two mechanisms of destruction: the water wave generated by the approximately 270 million m³ slide from Mount Toc first reached the village of Casso, located 260 m above the lake level in the opposite shore. Afterwards, the dam was over-topped by as much as 245 m. An estimated 30 million m³ of water then descended down the valley as a wave, initially more than 70 m height, destroying the villages of Longarone, Pirago, Villanova, Rivalta and Fae. About 2500 people were killed.

Fast landslides can also be triggered by external forces, such as by earthquakes. This is the case of the 1958 slide in the Lituya Bay, Alaska [MILLER, 1960; SLINGERLAND, 1979]. Triggered by a 8.3 magnitude earthquake, an estimated volume of 30.6 million m³ of amphibole and biotite schists slid down to the Gilbert Inlet at the head of Lituya Bay, causing a huge wave. According to the trimline of forest destruction, including tree uprooting and overturning, and erosion down to bedrock over an spur located at the opposite side in the Gilbert Inlet, the wave ran up to an elevation of 524 m., see Figure 9a. Much of the rest of the shoreline of the Lituya Bay was subsequently denuded from 30 to 200 m altitude, by the steep water front.

To model the flow phenomena present in the impulse wave generation, such as the high speed impact, impulse flux transfer, flow separation and reattachment, cavity formation, slide deformation and penetration into the water, etc. and the wave propagation, the authors proposal is based on the solution of the Navier-Stokes equations, including the three fluids, or fluid-like, materials involved in the problem. This is achieved using two indicator functions that allow to assign the corresponding material properties to each spatial point in the domain: the fluid-to-fluid interface described by the zero level-set of the indicator function. Therefore, the approach used to solve the interface position problem is front capturing. For improving accuracy and also due to algorithmic requirements, these two functions are distance functions, i.e. their slope is equal to one.

In the experimental set-up of FRITZ [2001], the Gilbert Inlet was reproduced in a rectangular prismatic channel with dimensions based on undistorted Froude similarity, the resulting scale being 1:675. Considering the specific topographic situation of the Gilbert Inlet, FRITZ [2001] considered the lateral spreading of the impulse wave triggered by the landslide as limited. Therefore, it was expected that the 2-D physical model gave a good prediction of wave and run-up heights inside Gilbert Inlet.

The experimental set-up included a pneumatic rockslide generator. Moreover, in order to capture the rapidly evolving flow fields, interfaces and pha-

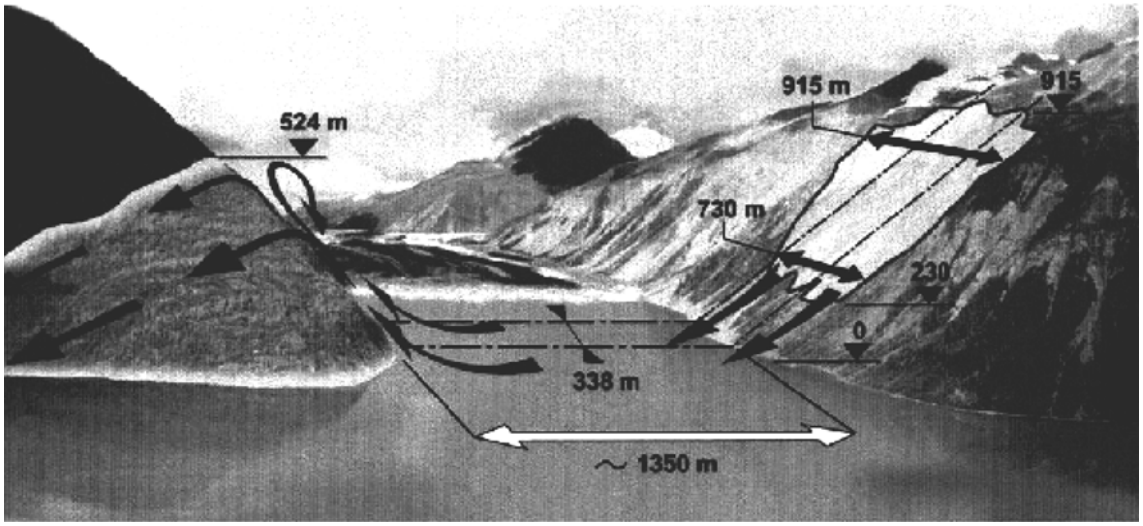

Fig. 9a – Gilbert Inlet illustration [from FRITZ *et al.*].
Fig. 9a – Illustrazione del canale Gilbert [da FRITZ et al.*].*

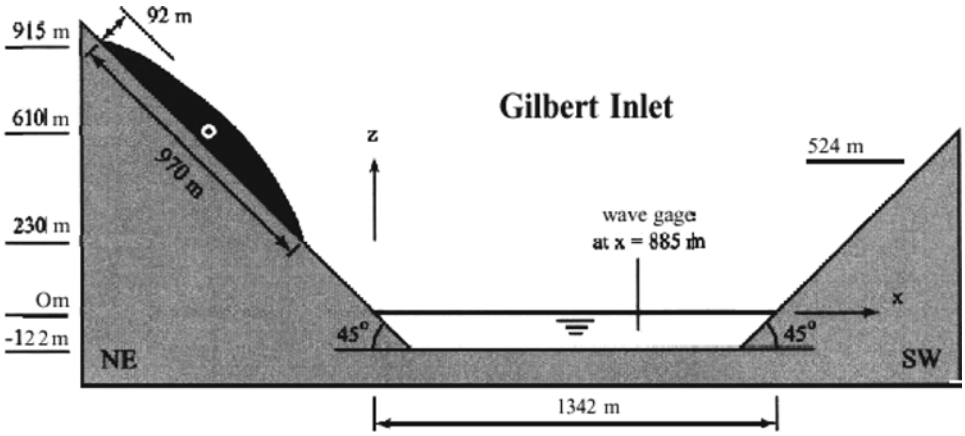

Fig. 9b – Simplified geometry of the Gilbert Inlet, basis of the physical and numerical model [from FRITZ *et al.*].
Fig. 9b – Geometria semplificata del canale Gilbert, base per la modellazione fisica e numerica [da FRITZ et al.*].*

ses mixing, the experimental set-up incorporated three different measurement devices: laser distance sensors (LDS), particle image velocimetry (PIV) and capacitance wave gages (CWG). In this way, the slide shape, impact time and velocity are available from the LDS and wave features from the CWG. Besides, a sequence of instantaneous velocity vector-fields were computed with the PIV.

Considering the level of the information provided by this physical model and that the results obtained agreed well with the field observations, it has been selected to check the performance of the proposed numerical procedure.

The simplified geometry of the Gilbert Inlet along the slide axis used by FRITZ (2001) as basis for the physical model, see Figure 9b, is also the basis for the numerical model. This domain has been meshed using the 7368 three nodes triangles and 3855 nodes depicted in Figure 10.

All the boundary is considered a frictionless and impermeable wall. A number of sensitivity calculations performed by the authors indicated that the friction law and the friction factor selected do not alter significantly the calculated results unless no-slipping is produced. It has also been checked that the open air boundary is far enough to leave basically unaffected the results on the area of concern.

The granular material used by Fritz in the physical model to simulate the landslide consisted of 87% Barium-Sulphate compounded with 13% Polypropilene resulting in a particle density of 2.64 t/m^3. This density matches the assumed schist density, 2.7 t/m^3. Fritz estimated the bulk density of this granular material as 1.61 t/m^3, considering a void fraction of 39% from data obtained on Alpine debris flows, however, it remains unknown to what extent the rockslide broke up before impacting into Gilbert Inlet and developed into a granular flow. As a bulk

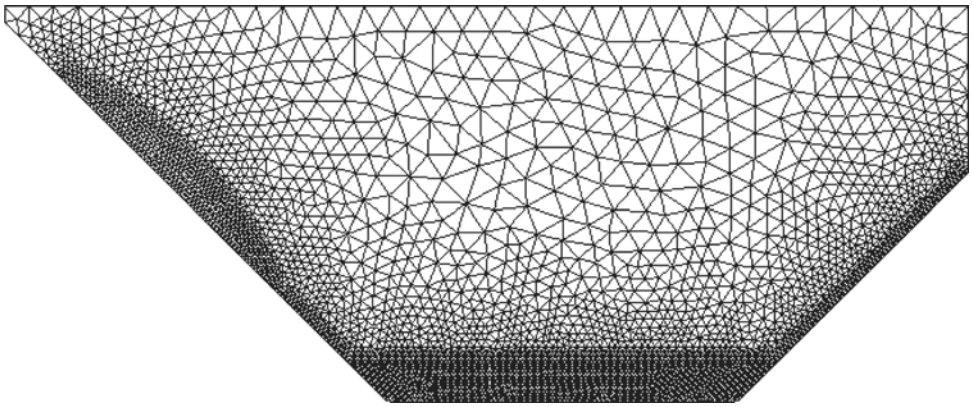

Fig. 10 – Mesh used to model the Gilbert Inlet along the slide axis. Boundary conditions are impermeable wall.
Fig. 10 – Maglia utilizzata per modellare il canale Gilbert lungo l'asse della colata. I contorni sono considerati impermeabili.

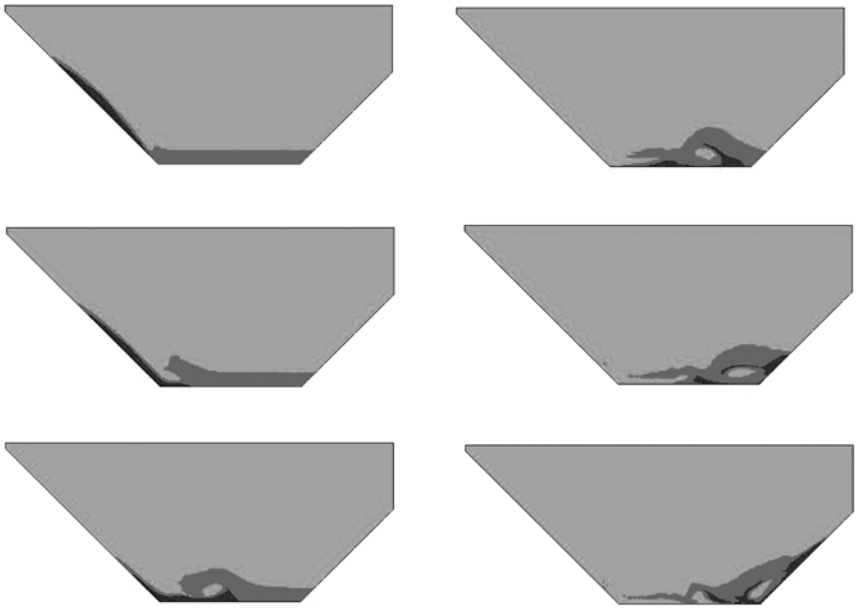

Fig. 11 – Evolution of the different phases due to the landslide impact calculated by the numerical model. Time increment is 5s. Bulk density of solid is 1.61 t/m^3.
Fig. 11 – Evoluzione delle differenti fasi dovute all'impatto, calcolate secondo il modello numerico. L'incremento temporale è pari a 5 s; la densità del solido è di 1.61 t/m^3.

density of 1.61 t/m^3 is used in the physical model, the authors have considered this value in the numerical model. Finally, as the internal friction angle of this material is unknown, the simulation done assumes it is zero.

Figure 11 presents a sequence of the landslide impact according to the numerical model and Figure 12 the corresponding from the physical model.

It is observed that the interfaces between the three fluids are sharp in the physical model, i.e. no mixing occurs during the first instants of the landslide impact as assumed in the numerical model. Later, in both the physical and numerical models, a large air cavity develops at the rear of the slide as its penetration velocity is larger than the wave velocity. This air cavity subsequently collapses during the slide run-out along the bottom, causing a significant air-water mixing. As the wave has already propagated outside the collapsing air bubble zone, the energy losses due to this energetic air-water mixing during the air bubble collapse may have a limited effect on the wave characteristics.

Table I summarizes the key results obtained in the physical and the numerical models. These results indicate that the initial instants of the slide impact and run out onto the bottom are well reproduced and they are only slightly dependent on the slide characteristics. It is noted, however, that the wave height at a position, 885 m, closer to the headland, see Figure 12, is overpredicted.

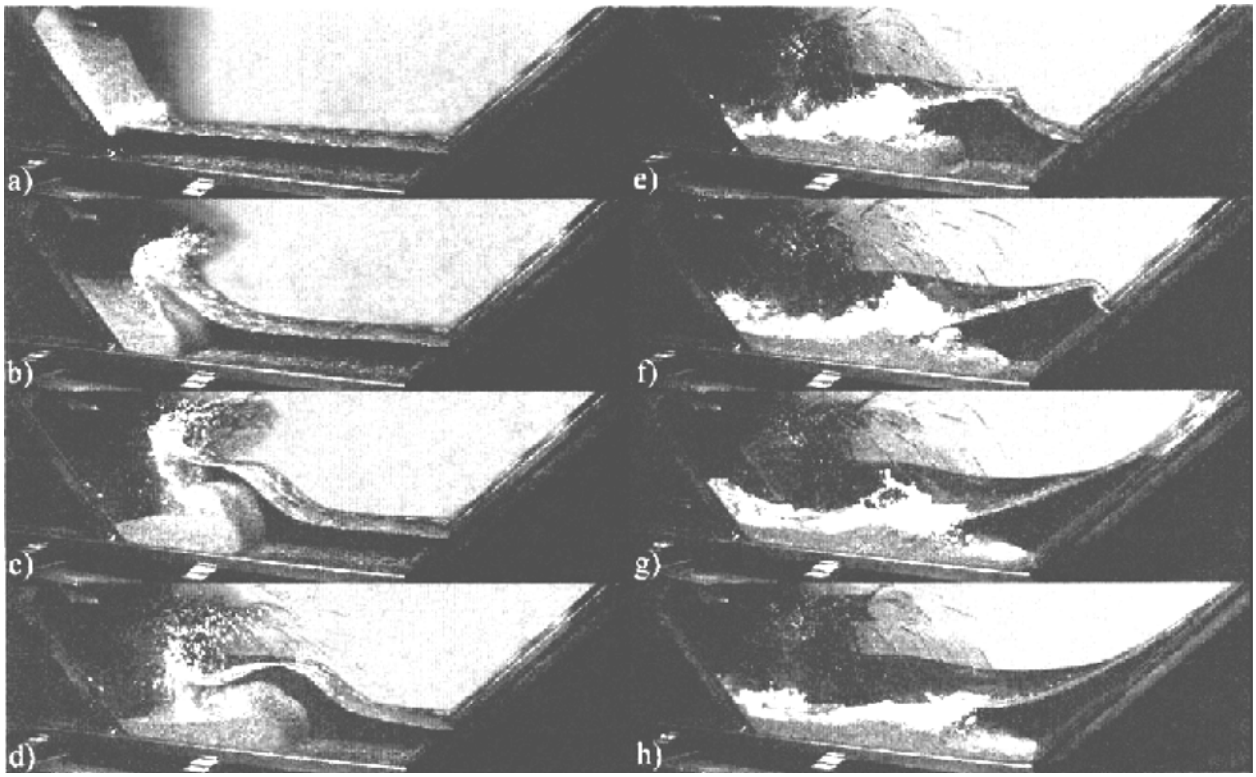

Fig. 12 – Photo-sequence of the granular slide impact experiment of FRITZ *et al.* Time increment is 5s.
Fig. 12 – Sequenza fotografica dell'impatto del corpo di frana nell'esperimento di FRITZ et al. *L'incremento temporale è pari a 5s.*

Tab. I – Measured and calculated wave characteristics.
Tab. I – Onde caratteristiche misurate e calcolate.

	Measured (FRITZ *et al.*)	Calculated
Slide duration (s)	7	10
Slide veloc. at impact (m/s)	110	101
Slide length at impact (m)	748	1039
Maximum wave height (m)	>200	193
Time for max. wave (s)	11	24
Max. wave position (m)	600	733
Total time (s)	42	35
Max. wave height at 885m	152	180
Time for max. wave at 885m (s)	16	26.8

This effect is attributed to a reduced energy dissipation in the numerical model. In effect, energy losses due to turbulence and phases mixing, which are not considered in the current numerical model, may further reduce the height elevation closed to headland.

5. Conclusions

This paper has presented a set of hierarchically structured mathematical models which can be used to reproduce fluidization processes occurring on fast catastrophic landslides, and some of their effects, such as waves in reservoirs, lakes and bays.

The key point is pore pressure generation and dissipation, which can explain the high velocities of propagation and long run out distances of such mass movements.

6. Acknowledgements

The authors gratefully acknowledge the finantial support of the Spanish Ministry of Science (Project ANDES REN 2001.0266.C02.01), the European Union (Project DIGA RTN 2001.00472), and the Spanish Agency of International Cooperation (AECI).

References

BIOT M.A. (1941) – *General theory of three-dimensional consolidation*. J.Appl.Phys. 12, pp. 155-164.

BIOT M.A. (1955) – *Theory of elasticity and consolidation for a porous anisotropic solid*. J.Appl.Phys., 26, pp. 182-185.

COUSSY O. (1995) – *Mechanics of Porous Media*. John Wiley and Sons, Chichester.

DARVE F., LAOUAFA F. (2001) – *Modelling of slope failure by a material instability mechanism*. Computers and Geotechnics, 29, pp. 301-325.

DIKAU R., BRUNDSEN D., SCHROTT L., IBSEN M.L. (2000) – *Landslide Recognition*. John Wiley and Sons, 1996.

DE BOER R. (2000) – *Theory of porous media*. Springer-Verlag, Berlin.

FEDKIW R.P., ASLAM T., MERRIMAN B., OSHER S. (1999) – *A non-oscillatory Eulerian approach to interfaces in multimaterial flows (the ghost fluid method)*. J. Comp. Phys., 152(2), pp. 457-492

FERNÁNDEZ MERODO J.A., PASTOR M., MIRA P., TONNI L., HERREROS M.I., GONZÁLEZ E., TAMAGNINI R. (2004) – *Modelling of diffuse failure mechanisms of catastrophic landslides*. Comp.Methods Appl. Mech.Engrg., 193, pp. 2911-2939.

FRITZ H.M., HAGER W.H., MINOR H.-W. (2001) – *Lituya bay case: Rockslide impact and wave run-up*. Science of Tsunami Hazards, 19(1), pp. 3-23.

HERREROS M.I., MABSSOUT M., PASTOR M. (2005) – *Application of Level-Set approach to moving interfaces and free surface problems in flow through porous media*. *Computer Methods in Applied Mechanics and Engineering*. In press, Available on line 10 March 2005.

HUNGR O. (1995) – *A model for the runout analysis of rapid flow slides, debris flows and avalanches*. Can.Geotech.J., 32, pp. 610-623.

HUTCHINSON J.N. (1986) – *A sliding-consolidation model for flow slides*, Can.Geotech.J., 23, pp. 115-126.

HUTTER K., KOCH T. (1991) – *Motion of a granular avalanche in an exponentially curved chute: experiments and theoretical predictions*. Phil. Trans. R. Soc.London, A, 334, pp. 93-138.

IVERSON R.I., DENLINGER R.P. (2001) – *Flow of variably fluidized granular masses across three dimensional terrain. 1. Coulomb mixture theory*. J.Geophys.Res. 106, n. B1, pp. 537-552.

JEYAPALAN J.K., DUNCAN J.M., SEED H.B. (1983) – *Investigation of flow failures of tailing dams*. J. Geotech. Engng., ASCE, 109, pp. 172-189.

JIN M., FREAD D.L. (1997) – *One-dimensional routing of mud/debris flows using NWS FLDWAV model*, in C.L.Chen (Ed.), *Debris-Flow Hazards Mitigation: Mechanics, Prediction and Assessment*. *ASCE*, pp. 687-696.

LAKEHAL D., MEIER M., FULGOSI M. (2001) – *Interface tracking towards the direct simulation of heat and mass transfer in multiphase flows*. Int. J. Heat and Fluid Flow, 23, pp. 242-257.

LEWIS R.L., SCHREFLER B.A. (1998) – *The Finite Element Method in the Static and Dynamic Deformation and Consolidation of Porous Media*. J.Wiley and Sons.

MILLER D.J. (1960) – *Giant waves in Lituya Bay, Alaska*. Geological Survey Professional Paper 354-C. U.S. Goverment Printing Office, Washington D.C.

PASTOR M., TAMAGNINI C. (2002) – *Numerical Modelling in Geomechanics*. Revue Française du génie civil, vol. VI, Hermès-Lavoisier (Eds.), Paris.

PASTOR M., QUECEDO M., FERNÁNDEZ MERODO J.A., HERREROS Mª.I., GONZÁLEZ E., MIRA P. (2002) – *Modelling Tailing Dams and mine waste dumps failures*. Géotechnique, vol. LII, n. 8, pp. 579-592.

QUECEDO M., PASTOR M. (2003) – *Finite Element modelling of free surface flows on inclined and curved beds*. Journal of Computational Physics, vol. CLXXXIX, I, 1, pp. 45-62.

SAVAGE S.B., HUTTER K. (1991) – *The dynamics of avalanches of granular materials from initiation to runout*. Part I: Analysis, Acta Mechanica, 86, pp. 201-223.

SETHIAN J.A (1996) – *Level Set Methods. Evolving interfaces in geometry, fluid mechanics, computer vision, and material science*. Cambridge University Press.

SLINGERLAND R.L., VOIGHT B. (1979) – *Ocurrences, properties, and predictive models of landslide-generated water waves*, Developments in geotechnical engineering, 14B, Voight, B. (Eds.). Elsevier, Amsterdam, pp. 317-397.

SUSSMAN M., SMERAKA P., OSHER S. (1994) – *A level-set approach for computing solutions to incompressible two-phase flow*. J. Comp. Phys., 114, pp. 146-159.

VARDOULAKIS I., SOULEM J., (1995) – *Bifurcation Analysis in Geomechanics*, Blakie Academic & professional, 1995.

ZIENKIEWICZ O.C., CHANG C.T., BETTESS P. (1980) – *Drained, undrained, consolidating dynamic behaviour assumptions in soils*. Géotechnique 30, pp. 385-395.

ZIENKIEWICZ O.C., SHIOMI T. (1984) – *Dynamic behaviour of saturated porous media: The generalised Biot formulation and its numerical solution*. Int.J.Num.Anal.Meth.Geomech.,8, pp. 71-96.

ZIENKIEWICZ O.C., CHAN A.H.C., PASTOR M., PAUL D.K, SHIOMI T. (1990a) – *Static and dynamic behaviour of soils: a rational approach to quantitative solutions. I.* Fully saturated problems Proc.R.Soc.Lond. A 429, pp. 285-309.

ZIENKIEWICZ O.C, XIE Y.M., SCHREFLER B.A., LEDESMA A., BICANIC. N. (1990b) – *Static and dynamic behaviour of soils: a rational approach to quantitative solu-*

tions. II. Semi-saturated problems Proc.R. Soc.Lond. A 429, pp. 311-321.
ZIENKIEWICZ O.C., CHAN A.H.C., PASTOR M., SHREFLER B.A., SHIOMI T. (2000) – *Computational Geomechanics*. J.Wiley and Sons.

Modellazione di movimenti franosi rapidi e dei fenomeni ondosi indotti in bacini o altri corpi fluidi

Sommario

Alcune masse franose rapide, spesso catastrofiche, che si propagano per lunghe distanze mostrano un comportamento meccanico simile a quello di un fluido. La fluidificazione, o liquefazione, del terreno è causata dalla sua struttura molto sciolta, metastabile. La tendenza a densificare sotto azioni di taglio genera le elevate pressioni interstiziali responsabili di questo fenomeno. Si propone qui un modello che coglie l'accoppiamento tra lo scheletro solido e il fluido interstiziale, in grado di modellare sia la fase di innesco che di propagazione del fenomeno. Il modello è capace di riprodurre la dissipazione delle pressioni durante la fase di propagazione dell'onda. In generale è possibile poi semplificare il modello attraverso l'integrazione sulla verticale. Nel caso si mantenga invece la formulazione originale, diviene necessario descrivere l'interfaccia tra la massa in frana e l'aria atmosferica; ciò può essere ottenuto mediante un algoritmo di level set. Un vantaggio di questa formulazione è di rendere possibile anche la modellazione degli effetti della caduta di una frana in un lago, in un bacino artificiale o in una baia. Anche le altre interfacce (aria-terreno, aria-acqua e terreno-acqua) possono essere modellate mediante algoritmi di level set.